SECOND EDITION

Handbook of Laser Technology and Applications

VOLUME I

Lasers
Principles and Operations

edited by
Chunlei Guo • Subhash Chandra Singh

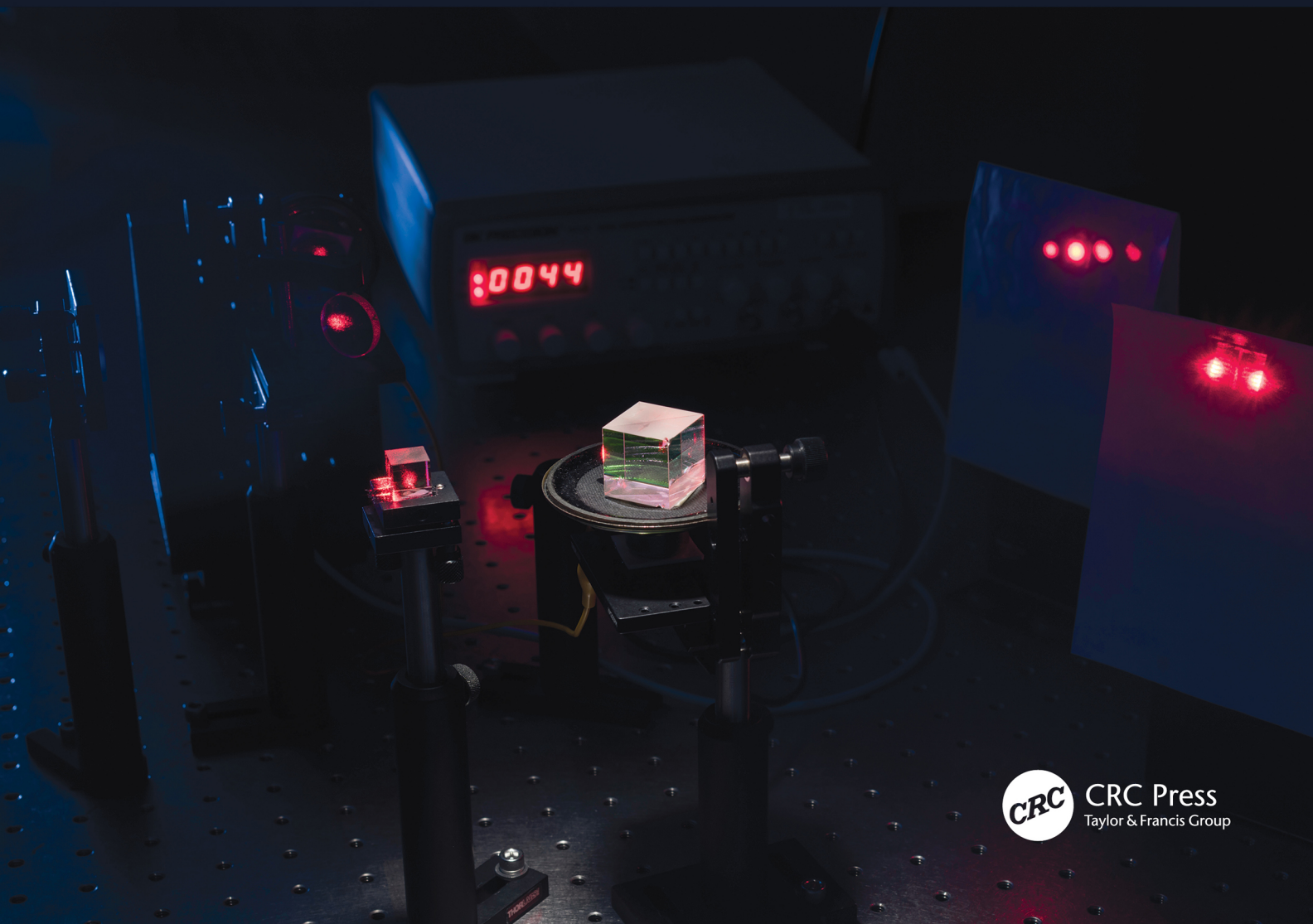

CRC Press
Taylor & Francis Group

Handbook of Laser Technology and Applications

Handbook of Laser Technology and Applications

Lasers: Principles and Operations (Volume One)
Second Edition

Lasers Design and Laser Systems (Volume Two)
Second Edition

Lasers Application: Material Processing and Spectroscopy (Volume Three)
Second Edition

Laser Applications: Medical, Metrology and Communication (Volume Four)
Second Edition

Handbook of Laser Technology and Applications

Lasers: Principles and Operations (Volume One)

Second Edition

Edited by
Chunlei Guo
Subhash Chandra Singh

CRC Press
Taylor & Francis Group
Boca Raton London New York

CRC Press is an imprint of the
Taylor & Francis Group, an **informa** business

Second edition published 2021
by CRC Press
6000 Broken Sound Parkway NW, Suite 300, Boca Raton, FL 33487-2742

and by CRC Press
2 Park Square, Milton Park, Abingdon, Oxon, OX14 4RN

First edition published by IOP Publishing 2004

CRC Press is an imprint of Taylor & Francis Group, LLC

Library of Congress Cataloging-in-Publication Data
Names: Guo, Chunlei, editor. | Singh, Subhash Chandra, editor.
Title: Handbook of laser technology and applications : four volume set /
[edited by] Chunlei Guo and Subhash Chandra Singh.
Description: 2nd edition. | Boca Raton : CRC Press, 2021- |
Series: Handbook of laser technology and applications | Includes bibliographical
references and index. | Contents: v. 1. Lasers: principles and operations —
v. 2. Laser design and laser systems — v. 3. Lasers applications: materials processing —
v. 4. Laser applications: medical, metrology a [?].
Identifiers: LCCN 2020037189 (print) | LCCN 2020037190 (ebook) |
ISBN 9781138032613 (v. 1 ; hardback) | ISBN 9781138032620 (v. 2 ; hardback) |
ISBN 9781138033320 (v. 3 ; hardback) | ISBN 9780367649173 (v. 4 ; hardback) |
ISBN 9781138196575 (hardback) | ISBN 9781315389561 (v. 1 ; ebook) |
ISBN 9781003127130 (v. 2 ; ebook) | ISBN 9781315310855 (v. 3 ; ebook) |
ISBN 9781003130123 (v. 4 ; ebook)
Subjects: LCSH: Lasers.
Classification: LCC TK7871.3 .H25 2021 (print) | LCC TK7871.3 (ebook) |
DDC 621.36/6—dc23
LC record available at https://lccn.loc.gov/2020037189
LC ebook record available at https://lccn.loc.gov/2020037190

ISBN: 9781138032613 (hbk)
ISBN: 9780367649692 (pbk)
ISBN: 9781315389561 (ebk)

Typeset in Times
by codeMantra

Contents

7

Nonlinear Optics

Orad Reshef and Robert W. Boyd

CONTENTS

7.1 Basic Concepts

Nonlinear optics is the study of the interaction of light with matter under conditions such that the linear superposition principle is not valid. The origin of this breakdown of the linear superposition principle can usually be traced to a modification of the optical properties of the material medium induced by the presence of an intense optical field. With a few exceptions [1], only laser light is sufficiently strong to lead to a significant modification of the optical properties of a material system and, for this reason, the field of nonlinear optics is basically the study of the interaction of laser light with matter. In this context, it is important to distinguish two different sorts of nonlinear optical effects: (i) effects associated with the nonlinear optical response of the material contained within the laser cavity itself; and (ii) effects induced by a prescribed laser beam outside of the laser cavity. In this chapter, we are concerned primarily with the second possibility, which constitutes the traditional field of nonlinear optics. Nonlinear optical processes occurring within the laser cavity itself constitute a central aspect of laser physics, as described in Chapter 1, and lead to important effects such as laser instabilities and chaos [2] and self-mode-locking of lasers [3]. The treatment of nonlinear optics presented in this chapter is necessarily limited in scope. More detailed treatments can be found in various monographs on the subject [4–10] as well as in the research literature. The present approach follows most closely the notational conventions of Ref. [5].

Nonlinear optical effects can often be described by assuming that the response of the material system can be expressed

as a power series expansion in the strength $\tilde{E}(t)$ of the applied laser field:

$$\begin{aligned}\tilde{P}(t) &= \chi^{(1)}\tilde{E}(t) + \chi^{(2)}\tilde{E}^2(t) + \chi^{(3)}\tilde{E}^3(t) + \ldots \\ &\equiv \tilde{P}^{(1)}(t) + \tilde{P}^{(2)}(t) + \tilde{P}^{(3)}(t) + \ldots,\end{aligned} \tag{7.1}$$

where $\tilde{P}(t)$ is the induced dipole moment per unit volume, *i.e.* the dielectric polarization. Here, the first term describes ordinary linear optics and includes the linear susceptibility $\chi^{(1)}$, the second term describes the second-order nonlinear optical effects and includes the second-order susceptibility $\chi^{(2)}$, *etc*. We shall see later that there is a significant qualitative difference between even- and odd-order nonlinear optical effects. To summarize these differences briefly, the crystal symmetry determines whether even orders are present within a material, and odd-order nonlinearities allow for processes where the output frequency is identical to an input frequency. We note that second-order nonlinear optical effects involve processes involving the simultaneous interaction of three photons, whereas third-order processes involve the interaction of four photons. Thus, second-order nonlinear optics includes processes such as second-harmonic generation (*i.e.* where two waves at a frequency ω combine to form a wave at a frequency of 2ω), sum- and difference-frequency generation and optical rectification (*i.e.* where a static field is generated under intense illumination); in contrast, third-order nonlinear optical effects include processes such as third-harmonic generation, the intensity dependence of the refractive index and four-wave mixing processes.

Typically, a nonlinear polarization of the type described in equation (7.1) is used as a source term in the driven wave equation:

$$\nabla^2\tilde{E} - \frac{\varepsilon}{c^2}\frac{\partial^2\tilde{E}}{\partial t^2} = \frac{1}{\varepsilon_0 c^2}\frac{\partial^2\tilde{P}^{NL}}{\partial t^2}. \tag{7.2}$$

Here, we are assuming that the material is lossless and dispersionless and that the slowly varying approximation holds. For different nonlinear processes, $\tilde{P}^{NL}$ is replaced with the appropriate field terms and nonlinear susceptibility tensor elements, which generates the corresponding nonlinear signal.

Equation (7.1) has been written in a highly simplified form. In general, the relation between the polarization and the applied laser field must treat the tensor nature of the nonlinear coupling and any possible frequency dependence of the nonlinear susceptibility elements. One particularly useful way of generalizing equation (7.1) to deal with such issues is to express $\tilde{P}(t)$ and $\tilde{E}(t)$ in terms of their frequency components as

$$\tilde{\boldsymbol{P}}(\boldsymbol{r},t) = \sum_n \boldsymbol{P}(\omega_n)\mathrm{e}^{-\mathrm{i}\omega_n t}\,\tilde{\boldsymbol{E}}(\boldsymbol{r},t) = \sum_n \boldsymbol{E}(\omega_n)\mathrm{e}^{-\mathrm{i}\omega_n t}, \tag{7.3}$$

where the summation extends over all positive and negative frequency components of the field. We then define the second-order susceptibility to be the coefficient relating the amplitude of the nonlinear polarization to the product of two field amplitudes according to

$$P_i(\omega_n + \omega_m) = \sum_{jk}\sum_{(mn)} \chi^{(2)}_{ijk}(\omega_n + \omega_m, \omega_n, \omega_m) E_j(\omega_n) E_k(\omega_m). \tag{7.4}$$

Here i, j and k refer to the Cartesian components of the fields, and the notation (nm) indicates that we are to sum over n and m while holding the sum $\omega_n + \omega_m$ fixed. By way of illustration, second-harmonic generation is described using these conventions by the susceptibility $\chi^{(2)}_{ijk}(2\omega,\omega,\omega)$, sum-frequency generation by the susceptibility $\chi^{(2)}_{ijk}(\omega_1+\omega_2,\omega_1,\omega_2)$ and difference-frequency generation by the susceptibility $\chi^{(2)}_{ijk}(\omega_1-\omega_2,\omega_1,-\omega_2)$. We similarly define the third-order susceptibility through the relation

$$\begin{aligned}P_i(\omega_0 + \omega_n + \omega_m) = \sum_{jkl}\sum_{mno} &\chi^{(3)}_{ijkl}(\omega_0 + \omega_n + \omega_m, \omega_0, \omega_n, \omega_m) \\ &\times E_j(\omega_0) E_k(\omega_n) E_l(\omega_m).\end{aligned} \tag{7.5}$$

Third-harmonic generation is then described by the susceptibility $\chi^{(3)}_{ijkl}(3\omega, \omega, \omega, \omega)$, and the intensity-dependent refractive index is described by $\chi^{(3)}_{ijkl}(\omega, \omega, \omega, -\omega)$. The intensity dependence of the refractive index is alternatively described in terms of the nonlinear refractive index coefficient n_2, defined by the relation

$$n = n_0 + n_2 I, \tag{7.6}$$

where I is the laser intensity, which is related to the nonlinear susceptibility through

$$n_2 = \frac{3}{4n_0\varepsilon_0 c\,\mathrm{Re}(n_0)}x^{(3)}. \tag{7.7}$$

It is often convenient to measure I in units of W m^{-2}, in which case n_2 is measured in units of m^2 W^{-1}. We then find that numerically

$$n_2\left(\frac{m^2}{W}\right) = \frac{283}{n_0\,\mathrm{Re}(n_0)}x^{(3)}\left(\frac{m^2}{v^2}\right). \tag{7.8}$$

In certain cases, n_2 is ill-defined, such as in low-index media where $n_2 I > n_0$. In these rare instances, $\chi^{(3)}$ becomes the preferred quantity with which nonlinear responses should be characterized [85].

7.2 Mechanisms of Optical Nonlinearity

In this section, we present a brief summary of the various physical mechanisms that can lead to a nonlinear optical response of a material system. We first make some general comments regarding the conditions under which various types of optical nonlinearities can occur.

7.2.1 Influence of Inversion Symmetry on Second-order Nonlinear Optical Processes

A well-known result states that the second-order susceptibility $\chi^{(2)}$ necessarily vanishes for a material possessing inversion symmetry. Thus, the second-order effects neither can occur in liquids, gases or glasses nor can they occur in any of the crystal classes that possess inversion symmetry.

7.2.2 Influence of Time Response on Nonlinear Optical Processes

It should be noted that only very fast physical mechanisms can lead to an appreciable response for processes in which the output frequency is different from the input frequencies, because, in order for such processes to occur, the material has to be able to respond at the difference frequencies of the various interacting fields. In contrast, processes such as the intensity-dependent refractive index can occur even as the consequence of sluggish mechanisms, because in this case, the average intensity of the incident light field can lead to a change of the refractive index. We thus conclude that only very fast processes can lead to processes such as harmonic generation.

7.2.3 Non-resonant Electronic Response

Perhaps, the most important source of optical nonlinearity is the response of bound electrons to an applied laser field. The electronic response can lead to both second- and third-order nonlinear optical processes. For the important case of non-resonant excitation, this mechanism has a very short response time. This response time can be estimated as the time required for the electron cloud surrounding the atomic nucleus to move in response to an applied laser field; this time is of the order of magnitude of the period associated with the motion of an electron in a Bohr orbit about the nucleus, which is of the order of magnitude of 10^{-16}s.

Non-resonant electronic response can be described theoretically in one of several ways. One is to solve Schrödinger's equation for an atom in the presence of an intense laser field and extract that part of the induced response which is second or third order in the amplitude of the applied field. Another is to develop a totally classical model of the optical response based, for instance, on adding nonlinear contributions to the restoring force introduced into the equation of motion used in the Lorentz model of the atom. These approaches lead to consistent predictions in relevant limits. At an even more elementary level, one can make order-of-magnitude estimates [4,11,12] of the size of the nonlinear optical response by arguing that the ratio of linear to nonlinear optical response will be of the order of $(E/E_{\mathrm{at}})^n$, where E_{at} is the characteristic atomic electric field strength and n is the order of the nonlinearity. Since $E_{\mathrm{at}} = m^2e^5/\hbar^4 = 5.14 \times 10^{11}\,\mathrm{V\,m^{-1}}$, this argument leads to the prediction that

$$\chi^{(2)} \sim \hbar^4/m^2\mathrm{e}^5 = 2\times10^{-12}\,\mathrm{m/V} \tag{7.9}$$

$$\chi^{(3)} \sim \hbar^8/m^4\mathrm{e}^{10} = 4\times10^{-24}\,\mathrm{m^2/V^2} \tag{7.10}$$

These values are in good order-of-magnitude agreement with the measured values for typical nonlinear optical materials.

7.2.4 Molecular Orientation

The molecular orientation effect occurs in anisotropic molecules and leads to a nonlinear optical response as a consequence of the tendency of molecules to become aligned along the electric field vector of the incident laser field. This process is illustrated in Figure 7.1. This alignment tends to increase the refractive index of the material, that is, it leads to a positive value of $\chi^{(3)}$. This process typically has a response time of the order of 1 ps and produces a nonlinear optical response of the order of $10^{-20}\mathrm{m^2V^{-2}}$. The contribution to the third-order susceptibility resulting from molecular orientation can be expressed as

$$\chi^{(3)} = \frac{4N}{135}\frac{(\alpha_3-\alpha_1)^2}{\kappa T}, \tag{7.11}$$

where N is the number density of molecules and $(\alpha_3 - \alpha_1)$ is the difference in polarizabilities along the principal dielectric axes of the molecule.

7.2.5 Electrostriction

Electrostriction is the tendency of materials to become compressed in the presence of a static or oscillating electric field. Since for most materials the refractive index increases with material density, this process leads to a positive value of $\chi^{(3)}$, typically of the order of $10^{-20}\mathrm{m^2V^{-2}}$. The response time of electrostriction is typically of the order of 1 ns. The contribution to the third-order susceptibility resulting from electrostriction can be expressed as

$$\chi^{(3)} = \frac{1}{3}\varepsilon_0 C_T \gamma_{\mathrm{e}}^2 \tag{7.12}$$

where C_{T} is the isothermal compressibility and where $\gamma_{\mathrm{e}} \equiv \rho\partial\varepsilon/\partial\rho$ is the electrostrictive constant.

7.2.6 Photorefractive Effect

The photorefractive effect [13,14] leads to a large nonlinear optical response but one that cannot usually be described in terms of a third-order (or any order) nonlinear susceptibility. The photorefractive effect occurs as a consequence of the

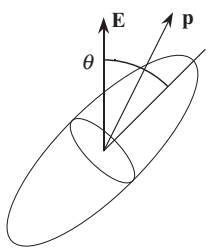

FIGURE 7.1 Origin of the molecular orientation effect, illustrating the tendency of an anisotropic molecule to become oriented in an electric field.

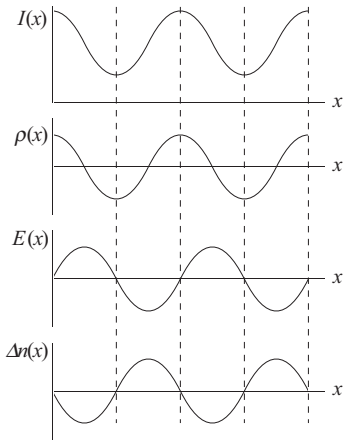

FIGURE 7.2 Origin of the photorefractive effect. $I(x)$ represents the spatially modulated laser intensity, $\rho(x)$ represents the free-charge distribution, $E(x)$ the static electric field created by this charge distribution and $\Delta n(x)$ is the resulting change in refractive index.

tendency of weakly bound electric charges within an optical material to migrate from regions of high intensity to regions of low intensity. This charge imbalance leads to the establishment of an electric field within the material, which modifies the refractive index of the material by means of the linear electro-optic (Pockels) effect. This basic process is illustrated in Figure 7.2. The photorefractive effect cannot be described in terms of a nonlinear susceptibility because the resulting change in refractive index tends to be independent of the strength of the incident laser field. Stronger laser fields tend to speed up the process of charge redistribution but do not change the final charge distribution. Typically, a laser beam of intensity 10 kW m^{-2} will produce a photorefractive response with a response time of the order of 1 s.

7.3 Nonlinear Optical Materials

The development of applications of nonlinear optics has historically been limited by the availability of materials with the required optical and environmental properties, and much effort has gone into the development of superior materials for use in nonlinear optics [15–17]. A brief representative sample of some materials of interest in second- and third-order nonlinear optics are given in Tables 7.1 and 7.2. More complete listings of material properties are to be found in various references [9,18–20]. A particularly useful approach towards the development of superior materials for nonlinear optics has been the development of nanocomposite materials or metamaterials [21–23,89–91].

TABLE 7.1

Properties of Several Second-Order Nonlinear Optical Materials

Crystal (class)	Transmission range (μm)	Refractive index (at 1.06 μm)	Nonlinear coefficient (pm V^{-1})
Silver gallium selenide $AgGaSe_2$ ($\bar{4}2m$)	0.78–18	$n_o = 2.7010$ $n_e = 2.6792$	$d_{36} = 33$ (at 10.6 μm)
β-barium borate BBO (3m)	0.21–2.1	$n_o = 1.6551$ $n_e = 1.5425$	$d_{22} = 2.3$ $d_{24} = d_{15} \leq 0.1$
Lithium iodate $LiIO_3$ (6)	0.31–5	$n_o = 1.8517$ $n_e = 1.7168$	$d_{31} = -7.11$ $d_{33} = -7.02$ $d_{14} = 0.31$
Lithium niobate $LiNbO_3$ (3m)		$n_o = 2.234$ $n_e = 2.155$	$d_{31} = -5.95$ $d_{33} = -34.4$
Potassium dihydrogen phosphate KH_2PO_4 (KDP)	0.18–1.55	$n_o = 1.4944$ $n_e = 1.4604$	$d_{36} = 0.63$
$KTiOPO_4$ KTP (mm^2)	0.35–4.5	$n_x = 1.7367$ $n_y = 1.7395$ $n_z = 1.8305$	$d_{31} = 6.5$ $d_{32} = 5.0$ $d_{33} = 13.7$ $d_{24} = 6.6$ $d_{15} = 6.1$

From a variety of sources including [19]. By convention, $d = \frac{1}{2}\chi^{(2)}$. The tensor nature of the nonlinear coefficients is expressed in contracted notation, in which the first index of d_{il} represents any of the three Cartesian indices and the second index l represents the product of two Cartesian indices according to the rule $l = 1$ implies xx, 2 implies yy, 3 implies zz, 4 implies yz or zy, 5 implies zx or xz and 6 implies xy or yx.

TABLE 7.2

Third-Order Nonlinear Optical Coefficients of Various Materials

Material	n_0	$\chi^{(3)}$ (m² V⁻²)	n_2 (m² W⁻¹)	Comments
Crystals				
Al_2O_3	1.8	3.1×10^{-22}	2.9×10^{-20}	
CdS	2.34	9.8×10^{-20}	5.1×10^{-18}	1.06 μm
Diamond	2.42	2.5×10^{-21}	1.3×10^{-19}	
GaAs	3.47	1.4×10^{-18}	3.3×10^{-17}	1,1.06 μm
Ge	4.0	5.6×10^{-19}	9.9×10^{-18}	THG $\lvert\chi^{(3)}\rvert$
LiF	1.4	6.1×10^{-23}	9.0×10^{-21}	
Si	3.4	2.8×10^{-18}	2.7×10^{-18}	THG $\lvert\chi^{(3)}\rvert$
TiO_2	2.48	2.1×10^{-20}	9.4×10^{-19}	
ZnSe	2.7	6.1×10^{-20}	3.0×10^{-18}	1.06 μm
Glasses				
Fused silica	1.47	2.5×10^{-22}	3.2×10^{-20}	
As_2S_3 glass	2.4	4.0×10^{-19}	2.0×10^{-17}	
BK-7	1.52	2.8×10^{-22}	3.4×10^{-20}	
BSC	1.51	5.0×10^{-22}	6.4×10^{-20}	
Pb Bi gallate	2.3	2.2×10^{-20}	1.3×10^{-18}	
SF-55	1.73	2.1×10^{-21}	2.0×10^{-19}	
SF-59	1.953	4.3×10^{-21}	3.3×10^{-19}	
Nanoparticles				
CdSSe in glass	1.5	1.4×10^{-20}	1.8×10^{-18}	non-res.
CS 3-68 glass	1.5	1.8×10^{-16}	2.3×10^{-14}	res.
gold in glass	1.5	2.1×10^{-16}	2.6×10^{-14}	res.
Polymers				
Polydiacetylenes				
PTS		8×10^{-18}	3×10^{-16}	non-res.
PTS		-6×10^{-16}	-2×10^{-14}	res.
9BCMU			1.9×10^{-14}	$\lvert n_2\rvert$, res.
4BCMU	1.56	-1.3×10^{-19}	-1.5×10^{-17}	non-res, $\beta = 1 \times 10^{-12}$ m W⁻¹
Liquids				
Acetone	1.36	1.5×10^{-21}	2.4×10^{-19}	
Benzene	1.5	9.5×10^{-22}	1.2×10^{-19}	
Carbon disulphide	1.63	3.1×10^{-20}	3.2×10^{-18}	$\tau = 2$ ps
CCl_4	1.45	1.1×10^{-21}	1.5×10^{-19}	
Diiodomethane	1.69	1.5×10^{-20}	1.5×10^{-18}	
Ethanol	1.36	5.0×10^{-22}	7.7×10^{-20}	
Methanol	1.33	4.3×10^{-22}	6.9×10^{-20}	
Nitrobenzene	1.56	5.7×10^{-20}	6.7×10^{-18}	
Water	1.33	2.5×10^{-22}	4.1×10^{-20}	
Other materials				
Air	1.0003	1.7×10^{-25}	5.0×10^{-23}	
Vacuum	1	3.4×10^{-41}	1.0×10^{-38}	
Cold atoms	1.0	7.1×10^{-8}	2×10^{-3}	(EIT BEC)
Fluorescein dye in glass	1.5	$2.8(1+\mathrm{i}) \times 10^{-8}$	$3.5(1+\mathrm{i}) \times 10^{-6}$	$\tau = 0.1$ s

Here n_0 is the linear refractive index. The third-order susceptibility $\chi^{(3)}$ is defined by equation (7.1). This definition is consistent with that introduced by Bloembergen [4]. In compiling this table, we have converted the literature values when necessary to the definition of equation (7.1). The quantity β is the coefficient describing two-photon absorption. Reference [24] provides an extensive tabulation of third-order nonlinear optical susceptibilities. Other references used are [25–36].

7.4 Optics in Plasmonic Materials

Plasmonic materials (e.g. metals) are materials where unbound electrons in the conduction band make a significant contribution to the optical properties of the material [86–88]. Though the motion of electrons is usually linked to dissipative losses, metals have been empirically shown to exhibit stronger nonlinearities than insulating or dielectric materials. Plasmonic materials also possess many other favourable properties for nonlinear effects, such as the possibility to confine light to sub-wavelength scales. This effect is associated with a large local field enhancement, known as the 'lightning rod effect', and under the correct circumstances, it can be quite dramatic. Consider, for example, a sphere with a dielectric constant ε embedded in a background of permittivity $\varepsilon_{\mathrm{BG}}$. If the sphere is placed in a uniform electric field of field strength E_0, the field within the sphere takes the value

$$E = \frac{3\varepsilon_{BG}}{\varepsilon + 2\varepsilon_{BG}} E_0. \tag{7.13}$$

This relation is valid in the quasi-static regime where the dimensions of the particle are smaller than the wavelength of an incoming light wave. The sphere enhances the electric field significantly if the real part of its permittivity is given by $\varepsilon = -2\varepsilon_{\mathrm{BG}}$, known as the Fröhlich criterion [92,93]. Since the real part of the permittivity of plasmonic materials is strongly frequency-dependent and can take negative values, this material can show large field-enhancement effects at the frequency where the real part of the denominator vanishes. The enhancement is ultimately limited by the imaginary component of the permittivity of the plasmonic medium; however, it remains substantial, and a field enhancement $|E/E_0|$ of one to two orders of magnitude is routinely achieved for gold nanoparticles of various shapes.

7.4.1 Linear Optical Properties

For photon energies below the threshold for inter-band transitions, the plasmonic materials may be accurately modelled using the Drude model, which yields a dielectric function of the form

$$\begin{aligned}\varepsilon(\omega) &= \varepsilon_\infty - \frac{{\omega_D}^2}{\omega^2 + i\gamma_D\omega} \\ &= \left(\varepsilon_\infty - \frac{{\omega_D}^2}{\omega^2 + {\gamma_D}^2}\right) + i\left(\frac{{\omega_D}^2\gamma D}{\omega\left(\omega^2 + {\gamma_D}^2\right)}\right)\end{aligned} \tag{7.14}$$

Here, ε_∞ is known as the high-frequency permittivity, γ_{D} is the electron damping term and ω_{D} is the plasma frequency. ε_∞ includes the residual polarization due to the positive background of the ion cores ($\varepsilon_\infty = 1$ for an ideal, undamped, free-electron gas, and usually $\varepsilon_\infty \lesssim 10$). The plasma frequency is the characteristic frequency at which a free-electron gas oscillates. It is given by

$$\omega_D \equiv \sqrt{\frac{Ne^2}{m^*\varepsilon_0}}, \tag{7.15}$$

where N is the free-electron volume density and m^* is the effective mass of the electron.

For a free-electron metal, this frequency also marks the metal/dielectric transition: as shown in equation (7.14), for frequencies significantly smaller than ω_{D}, the real part of ε becomes negative. Also, as the imaginary part scales with $1/\omega^3$, in this regime, it becomes large. Combined, these properties give the Drude material its metallic character. Near the plasma frequency, the real part of the permittivity takes small values, even crossing zero. Thus, the wavelength at which ω is equal to the plasma frequency is known as the epsilon-near-zero wavelength λ_{ENZ}. For solid conductors, the frequency of this zero-crossing is shifted to $\omega_D/\sqrt{\varepsilon_\infty}$, neglecting terms of order $(\gamma_D)^2$. This new frequency is known as the *shielded* plasma frequency.

At optical frequencies, the optical response of plasmonic materials exhibits significant deviations from the Drude model due to the onset of band-to-band transitions, even for what are traditionally considered 'good' metals (*e.g.* gold). These deviations can be accounted for by adding to the permittivity a series of Lorentz-oscillator terms, which are typically used to model bound electron effects [94]:

$$\varepsilon_L = -\sum_j f_j \frac{\omega_{L,j}^2}{\omega^2 + i\gamma_j\omega - \omega_{L,j}^2}. \tag{7.16}$$

Here, as for the Drude model in equation (7.14), each oscillator of index j represents the response of electrons harmonically oscillating at a resonance frequency of $\omega_{L,j}$ and a damping coefficient $\gamma_{L,j}$. The oscillator strength f_j is a unitless positive quantity bounded by unity. Though each of these coefficients holds a physical meaning, in the literature, they are typically treated as fitting parameters. Of note to our discussion earlier is that this contribution to the permittivity effectively shifts the epsilon-near-zero region for a given material so that it no longer depends solely on Drude coefficients.

7.4.2 Plasmonic Mechanisms of Optical Nonlinearity

Plasmonic materials exhibit some of the strongest observed ultrafast optical nonlinearities. The third-order nonlinear coefficients for a representative sample of these materials are given in Table 7.3. In addition to the aforementioned nonlinear mechanisms (*e.g.* molecular orientation, electrostriction, *etc.*), the plasmonic materials feature a few other important mechanisms of optical nonlinearity [95–98]:

- *Hot-electron nonlinearities.* Electrons can absorb heat from intense laser excitation. This absorption raises the free-electron temperature, changing the distribution of electrons in the band structure (also known as "Fermi smearing"), consequently modifying the effective mass of the electrons. Because these nonlinearities are thermal in origin, they are not instantaneous; however, they are typically the strongest and may still be ultrafast (*i.e.* possessing sub-picosecond rise and relaxation timescales).

TABLE 7.3

Third-Order Nonlinear Optical Coefficients of Selected Plasmonic Materials

Material	$\chi^{(3)}$ ($m^2\,V^{-2}$)	n_2 ($m^2\,W^{-1}$)	λ (nm)	Pulse width	Comments
Metals					
Ag	3.4×10^{-17}		396	28 ps	DFWM
Ag	2.8×10^{-19}		1060	ps	THG
Au	2.1×10^{-16}	2.6×10^{-14}	532	28 ps	DFWM
Au	$(-1.4+5i)\times10^{-16}$		532	30 ps	
Au	$(4.67+3.03i)\times10^{-19}$		796	100 fs	Kretschmann–Raether
Au	7.6×10^{-19}		1060	ps	THG
Nanoparticles					
Ag	7×10^{-15}		532	4.5 ps	
Au	1.7×10^{-15}		532	7 ns	DFWM
Au	9.1×10^{-15}		532	4.5 ps	
Cu		2×10^{-11}	532	100 ps	
Cu	$(1.4-3.5)\times10^{-16}$	$(2.0-4.2)\times10^{-14}$	570 – 600	6 ps	
Cu	3.8×10^{-14}		532	4.5 ps	
Cu	$(1.9-6.0)\times10^{-19}$		532	7 ns	
Cu		1.7×10^{-14}	770	130 fs	
Ni		5×10^{-15}	770	130 fs	
Pb		3×10^{-10}	532	100 ps	
Sn	2.1×10^{-14}		532	4.5 ps	
Transparent conducting oxides					
AZO	$(4+1i)\times10^{-20}$	3.5×10^{-17}	1310	100 fs	FWM ENZ region
ITO		6×10^{-18}	970	150 fs	
ITO		2.6×10^{-16}	1240	150 fs	AOI = 0° ENZ region
ITO	$(1.60+0.50i)\times10^{-18}$	1.1×10^{-14}	1240	150 fs	AOI = 60° ENZ region

Unless otherwise stated, the reported values were measured using a z-scan measurement [116,117]. Effective values for nanoparticle composites are distinguished from bulk material values, as various enhancement phenomena in small nanoparticles could account for many orders of magnitude difference in the reported values. References used are [85,101–115].

- *Conduction band filling.* Photons with energies larger than the inter-band transition are absorbed, promoting electrons from the valence band to the conduction band. For intense excitation, the conduction band gets filled, contributing to the nonlinear susceptibility largely in the form of saturable absorption.
- *Quantum-size effects.* Typically, intra-band transitions (*i.e.* due to electrons already in the conduction band) do not contribute to the nonlinear susceptibility; as free electrons experience no restoring forces, these bands contribute to the purely linear Drude response expressed in the equation (7.14) above. However, in small particles (*e.g.* <50 nm in diameter), nano-scale confinement leads to quantum-size nonlinear effects attributable to unbound electrons [99]. This nonlinearity is strongly size-dependent, scaling with the inverse of the particle volume.
- *Ponderomotive nonlinearities.* Certain metals (such as silver) also possess a ponderomotive nonlinearity. Here, charge carriers are repelled from high-intensity regions in the metal, depleting the electron density [100]. This effect manifests as a contribution to $\chi^{(3)}$ which looks like a highly dispersive ($\sim 1/\omega_4$) Kerr nonlinearity.

As a whole, this combination of nonlinear mechanisms exhibits a large dependence on laser parameters, such as the pulse duration and operating wavelength. This dependence is demonstrated explicitly in the large range of values reported for any single material listed in Table 7.3 and is discussed in greater detail for the case of gold in Ref. [97].

7.4.3 Epsilon-Near-Zero Nonlinearities

At the appropriate wavelength regime, hot-electron nonlinearities in particular can become quite important. Near their epsilon-near-zero wavelength, plasmonic materials possess intrinsic resonant properties that give rise to significant nonlinear optical effects. The origin of these large nonlinearities can be understood heuristically through the definition of the nonlinear refractive index coefficient n_2 defined in equation (7.7), where $n_2 \propto 1/(n\,\mathrm{Re}(n))$. As the real part of the refractive index is typically smallest when the permittivity vanishes, n_2 is expected to diverge in the epsilon-near-zero regime.

Upon intense laser excitation near the epsilon-near-zero wavelength, the unbound electrons in a plasmonic material are excited resonantly; the change in the effective electron mass is so significant that the plasma frequency is dramatically red-shifted, modifying the permittivity throughout the nearby spectrum, as described by equation 7.14. This frequency shift yields a broadband refractive index change Δ_n, which is largest where ε is the smallest once losses are taken into account (Figure 7.3).

The small magnitude of the permittivity in the ENZ region gives rise to another unique field enhancement mechanism. In the absence of a surface charge, the interface conditions ensure the continuity of the perpendicular component of the electric displacement field. Thus, the magnitude of the electric field $\vec{E}$ within a medium is proportional to the external field $\vec{E}_0$ and to the inverse of its permittivity:

$$\left|\vec{E}_\perp\right| \propto \frac{1}{\varepsilon}\left|\vec{E}_{0,\perp}\right| \tag{7.17}$$

Equation (7.17) leads to the following expression for the total field within a medium of permittivity ε for a given angle of incidence (AOI) θ:

$$\left|\vec{E}\right| = \left|\vec{E}_0\right|\sqrt{\cos^2\theta + \frac{\sin^2\theta}{\varepsilon}} \tag{7.18}$$

Therefore, for a small permittivity and at an oblique angle, the electric field within the medium can be much larger than the incident field. This additional enhancement mechanism helps to explain the angle-dependence of the nonlinear refractive index n_2 reported in Table 7.3.

Combining the effects of resonantly exciting unbound electrons, and the multiple-field enhancement mechanisms, plasmonic materials have made accessible an impressive new regime of ultrafast third-order nonlinear effects. The total change in refractive index Δn has even been shown to exceed the linear refractive index n [101]. Because of their large nonlinearities, these materials have once again become an active area of research and hold considerable promise towards making major technological advances in nonlinear photonic devices.

7.5 Second- and Third-harmonic Generation

Second-harmonic generation is the process in which an incident field at frequency ω_1 is converted to an output field at frequency $\omega_2 = 2\omega_1$ by means of the second-order response of the material system. This was, in fact, one of the first nonlinear optical processes to be studied in detail [37] and was discovered shortly after the invention of the laser. Second-harmonic generation can be a very efficient process, leading to conversion efficiencies approaching 100%. This process is described pictorially in Figure 7.4.

Second-harmonic generation can be described mathematically by introducing coupled-amplitude equations that describe the propagation of the fundamental and second-harmonic waves. We take the fundamental wave to have amplitude $A_1(z)\exp(\mathrm{i}k_1 z)$, where $k_1 = n_1\omega_1/c$ is its wavevector magnitude, and take the second-harmonic wave to have amplitude $A_2(z)\exp(\mathrm{i}k_2 z)$, where $k_2 = n_2\omega_2/c$ is its wavevector magnitude. The coupled amplitude equations are derived by introducing the nonlinear polarizations $P(2\omega) = \chi^{(2)}A_1^2\exp(2\mathrm{i}k_1)$ and $P(\omega) = 2\chi^{(2)}A_2A_1^*\exp\left[\mathrm{i}(k_2 - k_1)z\right]$ of equation (7.4) into the driven wave equation (equation 7.2) and then making the slowly varying amplitude approximation. The resulting equations have the form

$$\frac{dA_1}{dz} = \frac{i\omega_1^2\chi^{(2)}}{k_1c^2}A_2A_1^*\mathrm{e}^{-i\Delta kz} \tag{7.19}$$

and

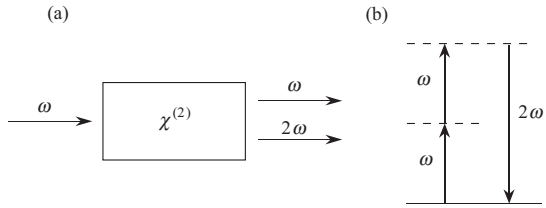

FIGURE 7.4 (a) The geometry of second-harmonic generation and (b) its description in terms of an energy-level diagram.

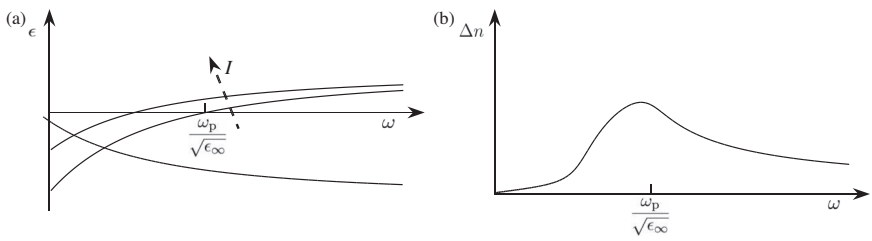

FIGURE 7.3 Hot-electron nonlinearities can lead to significant changes in optical properties. (a) Under intense laser excitation at the epsilon-near-zero wavelength, the plasma frequency is red-shifted as a function of pump intensity. (b) This red-shift may lead to a dramatic change in refractive index Δn.

$$\frac{dA_2}{dz} = \frac{i\omega_2^2\chi^{(2)}}{k_2c^2}A_1^2 e^{i\Delta kz}, \tag{7.20}$$

where $\Delta k = 2k_1 - k_2$. These equations express the fact that the amplitude of the second-harmonic wave is driven by the A_1^2 and that the generated second-harmonic wave acts back on the fundamental wave through the factor $A_2A_1^*$. Coupled amplitudes for other nonlinear optical processes are derived using analogous procedures.

Second-harmonic generation (and in fact all nonlinear processes) can only occur with good efficiency only if the wavevector mismatch factor Δk that appears in equations (7.12) and (7.13) is much smaller than the inverse of the length L of the interaction region. When this condition is met, the interaction is said to be phase-matched. Phase matching is typically achieved by making use of the natural birefringence of standard second-order nonlinear optical crystals and propagating the fundamental and second-order fields with orthogonal polarizations [38]. For $\Delta k = 0$, and assuming that only a fundamental field is present at the input to the medium, these equations can be solved exactly to find that

$$A_2(z) = \sqrt{n_1/n_2}\,A_1(0)\tanh(z/l) \tag{7.21}$$

where

$$l = \frac{\sqrt{n_1n_2c}}{\omega_1\chi^{(2)}|A_1(0)|}. \tag{7.22}$$

gives the characteristic distance over which the interaction occurs. Note that this model predicts that asymptotically the conversion efficiency can approach 100%. Second-harmonic generation in the plane-wave limit has been described more completely by Armstrong *et al*. [39], and the effects of laser-beam focusing on this process have been described by Boyd and Kleinman [40].

Radiation at the third-harmonic frequency can be created in one of two ways. One procedure is to create the third harmonic directly by means of a third-order interaction in which the amplitude of the nonlinear polarization is given by

$$P(3\omega) = \chi^{(3)}E(\omega)E(\omega)E(\omega). \tag{7.23}$$

Third-order interactions of this sort (and higher-order interactions, which give rise, for instance, to fifth- and seventh-harmonic generation) tend to be less efficient than second-order interactions but have the advantage that they can be used even at short wavelengths where standard nonlinear optical crystals are not transmitting. This approach to the generation of third-harmonic radiation has been described in detail by Ward and New [41] and by Miles and Harris [42].

The other approach to the generation of radiation at the third-harmonic frequency is to first generate a field at frequency 2ω through the process of second-harmonic generation followed by sum-frequency generation of the fields at frequencies ω and 2ω to produce an output at frequency 3ω. This approach can often be considerably more efficient than direct third-harmonic generation because lower-order processes tend to be stronger than third-order processes. In fact, through a judicious choice of experimental conditions, it is possible to produce radiation at the third-harmonic frequencies with efficiency exceeding 80% [43].

7.6 Optical Parametric Oscillation

An important technological application of nonlinear optics is the construction of parametric oscillators, which can produce tunable radiation over broad spectral regions spanning the infrared, visible and ultraviolet.

To understand the operation of an optical parametric oscillator (OPO), let us first examine the nature of the amplification that accompanies the process of difference frequency generation, which is illustrated in Figure 7.4. The left-hand side of this figure shows input waves at frequencies ω_3 and ω_2 with $\omega_3 > \omega_2$ incident on a second-order nonlinear optical material, within which the difference frequency wave at frequency $\omega_3 - \omega_2$ is generated. The energy-level diagram on the right-hand side of this figure reveals that one photon must be added to the field at frequency ω_2 for every photon that is created at frequency ω_1. The process of difference-frequency generation thus automatically leads to amplification of the lower-frequency input field (Figure 7.5).

This conclusion can be reached more rigorously by considering the coupled-waves equations describing the interaction of the two low-frequency waves in the presence of an undepleted pump wave at a frequency of ω_3,

$$\frac{dA_1}{dz} = \frac{i\omega_1^2\chi^{(2)}}{k_1c^2}A_3A_2^* e^{-i\Delta kz} \tag{7.24}$$

$$\frac{dA_2}{dz} = \frac{i\omega_2^2\chi^{(2)}}{k_2c^2}A_3A_1^* e^{i\Delta kz}, \tag{7.25}$$

where $\Delta k = k_3 - k_2 - k_1$. These equations can readily be solved for arbitrary boundary conditions. The solution for the special case of perfect phase matching ($\Delta k = 0$) and for no input at one of the lower frequencies (*i.e.* $A_2(0) = 0$) is given by

$$A_1(z) = A_1(0)\cosh\kappa z \Rightarrow \frac{1}{2}A_1(0)\exp(gz) \tag{7.26}$$

$$A_2(z) = i\left(\frac{n_1\omega_2}{n_2\omega_1}\right)^{1/2}\frac{A_3}{|A_3|}A_1^*(0)\sinh\kappa z \Rightarrow O(1)A_1^*(0)\exp(gz) \tag{7.27}$$

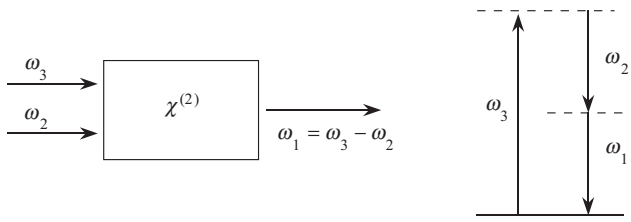

FIGURE 7.5 Illustration of the relation between difference frequency generation and optical parametric amplification. Note that amplification of the lower frequency input field ω_2 accompanies the creation of the difference frequency field ω_1.

where

$$g = \sqrt{k_1 k_2 k_j} = \frac{i\omega_j^2 \chi^{(2)} A_3}{k_j c^2}. \tag{7.28}$$

In these equations, the symbol $\Rightarrow$ denotes the asymptotic behaviour at large z and the symbol $O(1)$ denotes a number of the order of unity. Clearly, both waves asymptotically experience exponential growth.

The optical layout of an OPO is shown in Figure 7.6. Here, a pump wave of frequency ω_3 is incident on a second-order nonlinear optical crystal located inside an optical resonator. The end mirrors are assumed to be identical and to have reflectivities R_1 and R_2 at frequencies ω_1 and ω_2, respectively. The oscillator is said to be singly resonant if the end mirror reflectivity is large at either ω_1 or ω_2 and is said to be doubly resonant if the end mirror reflectivity is large at both ω_1 and ω_2. Generally speaking, doubly resonant oscillators have lower threshold pump intensities, but singly resonant oscillators are more readily operated in a stable manner because they do not require the independent establishment of a cavity resonance condition for the two separate frequencies ω_1 and ω_2.

Let us next consider the threshold condition for the establishment of oscillation in an OPO. For simplicity, we consider a simple model that applies to the doubly resonant oscillator. We assume that $R_1 = R_2 \approx 1$, that $\Delta k = 0$ and that the frequencies exactly meet the cavity resonance condition. The threshold condition can then be expressed as

$$\left(e^{2gL} - 1\right) = 2(1 - R). \tag{7.29}$$

Here, the left-hand side of the equation can be interpreted as the fractional energy gain per pass, and the right-hand side of the equation can be interpreted as the fractional energy loss per pass. The factor of two appears in the exponential because g is defined to be the amplitude gain coefficient. By expanding the exponential on the left-hand side to first order in gL, we find that the threshold condition can be expressed [44] as

$$gL = (1 - R). \tag{7.30}$$

Through the use of equation (7.28), we can use this result to determine the laser intensity required to reach the threshold for parametric oscillation.

The output frequencies of an OPO are usually controlled by adjusting the orientation of the nonlinear mixing crystal to determine which set of frequencies ω_1 and ω_2 (with $\omega_1 + \omega_2 = \omega_3$) satisfy the phase-matching condition ($\Delta k = 0$). OPOs tend to be broadly tunable because the tuning range is limited only by the limits of transparency of the crystal and by the limits over which the phase-matching relation can be established. Optical parametric oscillation was first observed experimentally by Giordmaine and Miller [44]. Continuous-wave OPO operation was first achieved by Smith *et al*. [45]. Early work on OPOs has been reviewed by Byer and Herbst [47]. An important material for the construction of OPOs is beta-barium borate [46].

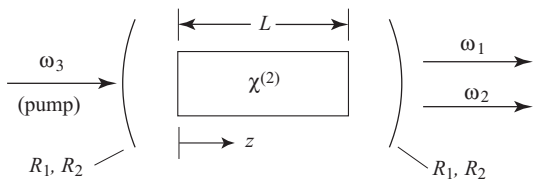

FIGURE 7.6 Layout of the OPO.

7.7 Optical Phase Conjugation

Optical phase conjugation [48–51] is a nonlinear optical process that has applications such as aberration correction, image processing and novel forms of interferometry [52]. The name phase conjugation derives from the fact that certain nonlinear optical processes have the ability to transform a field of the form

$$\tilde{E}(r,t) = A(r)e^{ikz - i\omega t} + c.c. \tag{7.31}$$

into the form

$$\tilde{E}_{pc}(r,t) = A^*(r)e^{-ikz - i\omega t} + c.c. \tag{7.32}$$

In addition to propagating in a direction opposite to that of the incident field, the wavefront of the phase-conjugate wave is changed from A to A^*. The nature of the phase-conjugation process is illustrated in Figure 7.7a, which shows an optical field falling onto a phase conjugating device which is often referred to as a phase conjugate mirror. The 'phase-conjugate' nature of this reversed wavefront allows it to remove, in double pass, the influence of aberrations in optical systems. The quantum statistical properties of the phase conjugation process have been described by Gaeta and Boyd [53].

The two primary means for forming a phase conjugate wavefront are degenerate four-wave mixing, which is illustrated in Figure 7.7b, and stimulated Brillouin scattering (SBS), which is illustrated in Figure 7.7c and will be discussed in further

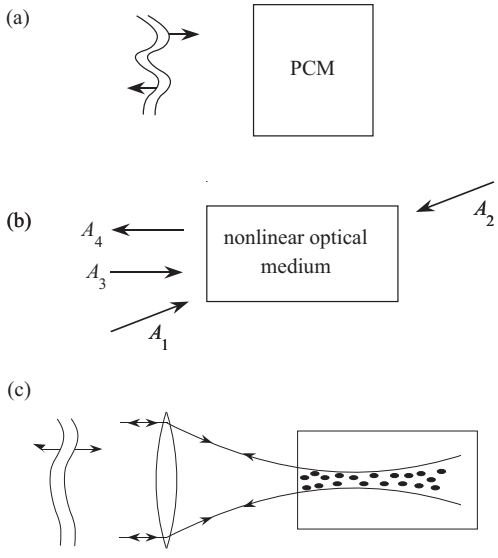

FIGURE 7.7 (a) Illustration of the nature of the phase-conjugation process, (b) phase conjugation by degenerate four-wave mixing and (c) phase conjugation by SBS.

detail later in the chapter. In the four-wave mixing interaction, a signal beam of amplitude A_3 interacts with two counter-propagating plane-wave pump beams of amplitudes A_1 and A_2 in a third-order nonlinear optical medium. Under these conditions, the dominant phase-matched contribution to the nonlinear optical susceptibility is of the form

$$P_{NL}(\omega_1) = 3\varepsilon_0 \chi^{(3)}(\omega_1, \omega_1, \omega_2, -\omega_2) A_1(\omega_1) A_2(\omega_2) A_3^*(\omega_2). \tag{7.33}$$

Here, ω_1 may be at the same frequency as ω_2. Since the nonlinear polarization is proportional to A_3^*, it will generate an output field that is the phase conjugate of the input field, that is a field proportional to A_3^*. The mutual interaction of the signal and conjugate beams can be described by the coupled amplitude equations

$$\frac{dA_3}{dz} = i\kappa A_4^* \quad \frac{dA_4}{dz} = i\kappa A_3^* \tag{7.34}$$

where the solution to these equations for the boundary conditions appropriate to the situation illustrated shows that the amplitude of the generated conjugate field is given by

$$A_4(0) = A_3^*(0) \frac{i\kappa}{|\kappa|} \tan|\kappa| L. \tag{7.35}$$

We see that the generated field is indeed proportional to the complex conjugate of the input field. We also see that a phase-conjugate mirror can have a reflectivity greater than 100%, because the pump waves provide energy to the phase-conjugate wave.

The other standard configuration for forming a phase-conjugate wavefront is through SBS, as illustrated in Figure 7.6c. SBS is described in more detail in Section 7.12 of this chapter. This process leads to phase conjugation because an aberrated input wave will produce a highly non-uniform volume intensity distribution in the focal region. The gain coefficient of the SBS process is proportional to the laser intensity, and the resulting non-uniform gain distribution will tend to generate an output wave whose wavefronts match those of the input wave.

7.8 Self-focusing of Light

Self-focusing is an example of a self-action effect of light. Other examples of self-action effects include self-trapping of light and the break-up of a beam of light into multiple filaments. These effects are illustrated schematically in Figure 7.8. These particular self-action effects can occur only if the nonlinear refractive index coefficient n_2 is positive. Self-focusing (Figure 7.8a) occurs because the refractive index at the centre of the laser beam is larger than in the wings of the laser beam. This effect causes the material medium to act like a positive lens, bringing the light to a focus within the material medium. Self-trapping (Figure 7.8b) occurs when the tendency of a beam to converge because of self-focusing precisely compensates for the tendency of the beam to diverge due to

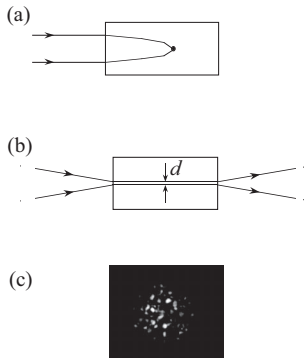

FIGURE 7.8 Several self-action effects of light are illustrated: (a) self-focusing, (b) self-trapping of light and (c) the break-up of a beam of light into multiple filaments.

diffraction effects. Simple arguments [5,54] show that this balance can occur only if the laser beam carries the critical power

$$P_{cr} = \lambda^2 / 8 n_0 n_2. \tag{7.36}$$

As a point of reference, P_{cr} has the value 30 kW for carbon disulphide at a wavelength of 700 nm. Self-trapped filaments are also known as spatial solitons. The use of spatial solitons has been proposed for optical switching applications [55]. According to the simple model leading to equation (7.36), self-trapped filaments can have any diameter d, as long as the total power contained in the beam has the value P_{cr}. Only if the power of the laser beam exceeds P_{cr}, self-focusing can occur. It is readily shown [5], on the basis of Fermat's principle, that the distance from the entrance face of the nonlinear material to the self-focus is given by

$$z_f = \frac{2n_0}{0.61} \frac{\omega_0^2}{\lambda} \frac{1}{(P/P_{cr} - 1)^{1/2}} \tag{7.37}$$

where ω_0 is the beam diameter. If the laser power is much greater than P_{cr}, another process known as filamentation (Figure 7.7c) can occur. In this process, the beam breaks up into multiple small filaments, each of which carries power P_{cr}. The origin of this process is that small perturbations on the incident laser wavefront experience exponential spatial growth as the consequence of near-forward four-wave mixing processes [56]. The maximum value of this growth rate is given by $g = (\omega/c) n_2 I$ and it occurs at the characteristic filamentation angle $\theta_{max} = \sqrt{2} g/k$. Filamentation is an undesirable process, and methods to suppress filamentation include the use of spatial filtering to remove aberrations from the laser wavefront, the use of specially structured beams [57] and the use of quantum interference effects [58] to eliminate the nonlinear response leading to filamentation.

7.9 Optical Solitons

Optical solitons are beams of light that propagate without changing their form, that is, they propagate as a self-similar solution to the wave equation [59]. By a *temporal soliton*, one means a

pulse of light that propagates through a dispersive medium with no change in shape because of a balancing of dispersive and nonlinear effects. By a *spatial soliton*, one means a beam of light that propagates with a constant transverse profile because of a balance between diffraction and self-focusing effects. Similarly, a *spatio-temporal soliton* is a pulse that propagates without spreading in time or in the transverse directions.

The basic equation describing the propagation of optical solitons is a generalization of the so-called nonlinear Schrödinger equation and has the form

$$\frac{\partial A}{\partial z}+\frac{1}{v_g}\frac{\partial A}{\partial t}+\frac{i\beta}{2}\frac{\partial^2 A}{\partial t^2}+\frac{1}{2ik}\nabla^2{}_T A = i2n_0\varepsilon_0 n_2\omega_0|A|^2 A \tag{7.38}$$

where $\vartheta_g \equiv \beta_1 = (\partial k/\partial\omega)^{-1}$ is the group velocity, $\beta_2 = \partial^2 k/\partial\omega^2$ is a measure of the dispersion in the group velocity, ∇_T^2 is the transverse Laplacian and ω_0 is the central frequency of the pulse. The term involving β_2 describes the tendency of the pulse to spread in time due to dispersive effects, the term involving ∇_T^2 describes diffraction and the term involving n_2 describes self-phase modulation and self-focusing effects. The propagation of temporal solitons can be described by this equation by discarding the transverse Laplacian, and the propagation of spatial solitons can be described by this equation by discarding the time derivatives. This equation possesses solutions relevant to many different physical situations. For instance, it possesses solutions in the form of bright solitons (*e.g.* a bright pulse on a zero background) or dark solitons (a decrease in intensity in an otherwise uniform non-zero background). Optical solitons can occur only for certain values of the material parameters. For instance, bright temporal solitons can occur only if n_2 and β_2 have opposite signs, and dark temporal solitons can occur only if these quantities have the same sign. Similarly, bright spatial solitons can occur only if n_2 is positive, whereas dark spatial solitons can occur only if n_2 is negative. Only certain solutions to equation (7.38) are stable to small perturbations. For instance, bright spatial solitons are stable in one transverse dimension but are unstable in two transverse dimensions.

A particularly important example of optical solitons is bright temporal solitons propagating through an optical fibre. The solution to equation (7.38), with the transverse terms discarded, that describes this occurrence is given by

$$A_s(z,\tau) = A_s^0 \mathrm{sech}(\tau/\tau_0)\mathrm{e}^{\mathrm{i}\kappa z}, \tag{7.39}$$

where $\tau = t - z/v_g$ and where the pulse amplitude A_S^0 and pulse width τ_0 must be related according to

$$\left|A_s^0\right|^2 = \frac{-\beta_2}{2n_0\epsilon_0\, n_2\omega_0\tau_0^2} \tag{7.40}$$

and where $k = -\beta_2/2\tau_0^2$ represents the phase shift experienced by the pulse upon propagation. Note that the condition (7.40) shows that β_2 and n_2 must have opposite signs in order for equation (7.39) to represent a physical pulse in which the intensity $\left|A_S^0\right|^2$ and the square of the pulse width τ_0^2 are both positive. We can see from equation (7.38) that, in fact, β_2 and γ must have opposite signs in order for group velocity dispersion to compensate for self-phase modulation.

For the case of an optical fiber, n_2 is positive with a value of approximately $3.2 \times 10^{-20}\mathrm{m}^2\ \mathrm{W}^{-1}$. Bright optical solitons can then occur only if β_2 is negative, and consideration of the dispersion of the refractive index of silica glass shows that β_2 is negative only at wavelengths longer than 1.3 μm. Optical solitons of this sort have been observed experimentally [60].

7.10 Optical Bistability

Optical bistability refers to the possibility that a given optical system may possess two (or more) outputs for a given input. This possibility was first described theoretically by Szöke *et al.* [64] and first observed experimentally by Gibbs *et al.* [62]. Extensive treatments of bistability can be found in Ref. [61,63]. The realization that optical bistability can occur is important because it suggests that nonlinear optical techniques can be used to perform logical operations similar to those of electronic digital computers.

A standard design for a bistable optical device and its typical operating characteristics are shown in Figure 7.9. Here, a wave of amplitude A_1 is shown falling onto a device in the form of a Fabry–Pérot interferometer filled with a third-order nonlinear optical material. Such a device can be bistable in the sense that, under certain situations, there can be more than one output intensity for a given input intensity. The theoretical analysis of such a device proceeds by deriving a relation between the input amplitude A_1 and the output amplitude A_3. The result is the well-known Airy equation

$$A_3 = \frac{T^2 A_1}{1 - R^2\mathrm{e}^{2ikL-\alpha L}}, \tag{7.41}$$

where T is the amplitude transmittance of either end mirror and R is the amplitude reflectivity. Here k is the total propagation constant and α is the total intensity absorption coefficient of the material within the resonator, including both their linear and nonlinear contributions. A nonlinear contribution to k or α or both can lead to bistable behaviour. As an illustration, if

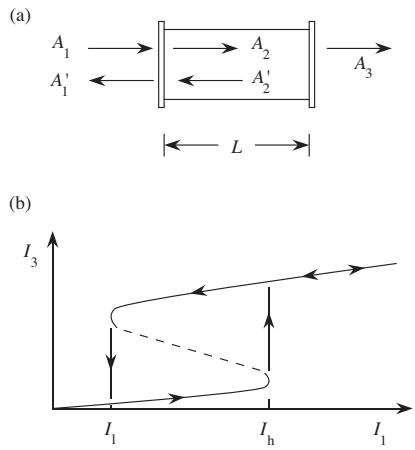

FIGURE 7.9 (a) Standard design for a bistable optical device and (b) typical operating characteristics.

we assume that the material within the resonator is a saturable absorber, for which the absorption coefficient α changes with intensity according to

$$\alpha = \frac{\alpha_0}{1 + I/I_s} \tag{7.42}$$

where I_s is the saturation intensity, we find that the output intensity $I_3 = |A_3|^2$ is related to the input intensity $I_1 = |A_1|^2$ according to

$$I_1 = I_3\left(1 + \frac{C_0}{1 + 2I_3/TI_s}\right)^2 \tag{7.43}$$

where $C_0 = R\alpha_0 L/(1 - R)$. Under certain conditions (in particular, for $C_0 > 8$), this equation predicts the occurrence of optical bistability. The input–output characteristics of the device under these conditions are illustrated schematically in Figure 7.8b. This curve has the form of a standard hysteresis loop and shows that, over a considerable range of input intensities, more than one output intensities can occur.

7.11 Optical Switching

Optical switching refers to the use of nonlinear optical methods to control the amplitude or propagation direction of one beam of light using a second beam of light. Early reviews that tended to define this field are given in Refs. [65] and [66].

A prototypical design for an all-optical switch is shown in Figure 7.10. In this design, a third-order nonlinear optical material is placed in one arm of a Mach–Zehnder interferometer. Let us first analyse the operation of such a device in the absence of an applied control field. The relative phase of the two pathways through the interferometer changes with signal wave input intensity according to $\phi_{NL} = n_2(\omega/c)IL$, and thus, the input can be directed either towards output port 1 or port 2 depending upon the input intensity. The threshold intensity for switching from one output port to the other is given by the condition that the nonlinear phase shift ϕ_{NL} is equal to π radians. In this configuration, the nonlinear interferometer could be used to separate low-intensity pulses from high-intensity pulses in a pulse train of variable intensity. More sophisticated types of switching behaviour can be obtained by applying an additional input field to the control port of the interferometer. For instance, the presence or absence of a control field can be used to direct the signal field either to output port 1 or port 2, so that the device would operate as a router.

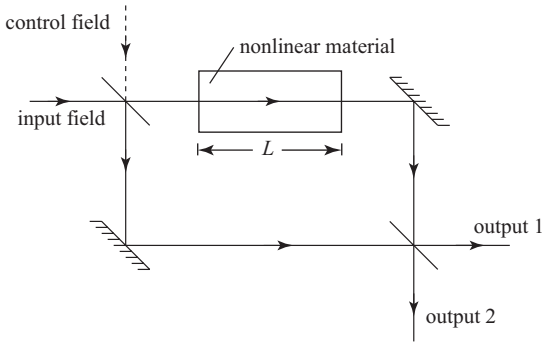

FIGURE 7.10 Typical design of an all-optical switching device, in the form of a nonlinear Mach–Zehnder interferometer.

7.12 Stimulated Light Scattering

The scattering of light can occur either as a consequence of spontaneous or stimulated processes. The distinction between these two types of light-scattering processes can be understood by noting [67] that all light scattering occurs as a consequence of localized fluctuations in the optical properties of the material medium. From this perspective, spontaneous light scattering occurs as a consequence of fluctuations induced by thermal or by quantum mechanical zero-point fluctuations, and stimulated light scattering occurs as a consequence of fluctuations that are induced by the presence of the laser field.

It is believed that all spontaneous light-scattering processes possess a stimulated analogue, and quantitative models have been presented that relate the optical coefficients of these two types of processes [68]. Some of the important light-scattering processes are summarized in Table 7.4.

7.12.1 Stimulated Raman Scattering

Stimulated Raman scattering (SRS) [69] is characterized by exponential growth of a light wave at the Stokes sideband of the laser field. In particular, in this process, the intensity $I_S(t)$ of a beam of light at the Stokes frequency $\omega_S = \omega_L - \omega_v$, where ω_L is the laser frequency and ω_v is the vibrational frequency of the molecule, increases with propagation distance z according to

$$I_S(z) = I_S(0)e^{gI_L z} \tag{7.44}$$

TABLE 7.4

Summary of Light-Scattering Processes

Process	Spectral Shift (m^{-1})	Line Width (m^{-1})	Gain ($m\ W^{-1}$)	Scattering Mechanism
Rayleigh scattering	None	5×10^{-2}	10^{-12}	Non-propagating density fluctuations
Rayleigh-wing scattering	None	10^3	10^{-11}	Fluctuations in the orientation of anisotropic molecules
Brillouin scattering	30	0.5	10^{-10}	Propagating sound waves
Raman scattering	10^5	500	5×10^{-11}	Vibrational modes of the molecules that constitute the scattering medium

where g is the Raman gain and I_L is the laser intensity. The Raman gain coefficient for various materials is given in Table 7.5. The Stokes shift for SRS is sufficiently large that SRS is an important technique for laser frequency shifting [70]. This nonlinear process was the one employed to create the first integrated continuous wave silicon lasers, since silicon cannot show optical gain based on normal stimulated emission in that it does not have a direct bandgap [118].

SRS can be understood by assuming that the optical polarizability $\alpha(t)$ of a molecule depends on the inter-atomic separation $q(t)$ according to

$$\alpha(t) = \alpha_0 + \left(\partial\alpha/\partial q\right)_0 \left[q(t) - q_0\right] \tag{7.45}$$

where q_0 is the equilibrium value of the inter-atomic separation [71]. Note that a periodic oscillation of $q(t)$ will produce a periodic oscillation of $\alpha(t)$ and consequently of the refractive index $n(t)$. Such a periodic modulation of $n(t)$ will tend to amplify light at a frequency detuned from the laser frequency by the vibrational frequency. Moreover, the simultaneous presence of the laser and Stokes beams will tend to reinforce the molecular vibration at the beat frequency of the waves. This process leads to exponential growth of the Stokes sideband, with a gain factor given by

$$g = \frac{i \in_0 N_{\omega S}}{4m\omega_\vartheta n S^c} \frac{(\partial a/\partial q)_0^2}{[\omega_s - (\omega_L - \omega_\vartheta)] + i\gamma} \tag{7.46}$$

where m is the reduced nuclear mass, γ is the vibrational damping rate and n_S is the refractive index at the Stokes frequency.

7.12.2 Stimulated Brillouin Scattering

The analysis of SBS shares many features in common with that of SRS but differs in the significant manner that SBS involves a collective excitation of the material medium. Consequently, the properties of SBS can be quite different in different directions. Our analysis here is restricted to geometries in which the laser and Stokes fields propagate in opposite directions.

The nature of the gain of the SBS process can be understood from the following perspective. The laser and counter-propagating Stokes waves beat together and, by means of the electrostrictive response of the material, produce a sound wave at the beat frequency which travels in the direction of the laser field. Some of the laser light then scatters from this sound wave and, in doing so, becomes Stokes-shifted and consequently reinforces the Stokes wave. But since the Stokes wave is now stronger, it tends to produce a stronger sound wave, and in this manner, the growth of the sound and Stokes wave mutually reinforce each other. These phenomena are illustrated in Figure 7.11. A consistent analysis of this situation shows that the Stokes wave experiences exponential amplification according to

$$I_S(z) = I_S(0)e^{g_0 I_L} \tag{7.47}$$

where the Brillouin gain factor is given by

$$g_0 = \frac{\gamma_e^2 \omega^2}{n\upsilon c^3 \rho_0 \Gamma_B} \tag{7.48}$$

and where γ_e is the electrostrictive constant introduced earlier in equation (7.12), ω is the laser frequency, n is the refractive index, υ is the velocity of sound, ρ_0 is the mean material density and Γ_B is the phonon-damping rate. The properties of SBS for several materials are summarized in Table 7.6.

TABLE 7.5

Properties of SRS for Several Materials

Substance	Frequency Shift (m^{-1})	Gain Factor g (m GW^{-1})
Liquids		
Benzene	99 200	0.03
Water	329 000	0.0014
Nitrogen	232 600	0.17
Oxygen	155 500	0.16
Gases		
Methane	291 600	0.0066 at 10 atm
Hydrogen	415 500 (vibrational)	0.015 (10 atm and above)
	45 000 (rotational)	0.005 (0.5 atm and above)
Deuterium	299 100 (vibrational)	0.011 (10 atm and above)
Nitrogen	232 600	7.1×10^{-4} (at 10 atm)
Oxygen	155 500	1.6×10^{-4} (at 10 atm)

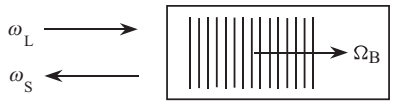

FIGURE 7.11 Illustration of the nature of SBS.

TABLE 7.6

Properties of SBS for a Variety of Materials[a]

Substance	$\Omega_B/2\pi$ (MHz)	$\Gamma_B/2\pi$ (MHz)	g_0 (m GW^{-1})
CS_2	5850	52.3	1.5
Acetone	4600	224	0.2
Toluene	5910	579	0.13
CCl_4	4390	520	0.06
Methanol	4250	250	0.13
Ethanol	4550	353	0.12
Benzene	6470	289	0.18
H_2O	5690	317	0.048
Cyclohexane	5550	774	0.068
CH_4 (1400 atm)	150	10	1
Optical glasses	15 000–26 000	10–106	0.04–0.25
SiO_2	25 800	78	0.045

[a] Values are quoted for a wavelength of 0.694 μm. To convert to other laser frequencies ω, recall that Ω_B is proportional to ω, Γ_B is proportional to ω^2 and g_0 is independent of ω.

7.13 Multi-photon Absorption

Multi-photon absorption refers to optical processes in which more than one photon is removed from the optical field in a single optical transition. Some typical multi-photon absorption processes as well as normal one-photon absorption are shown

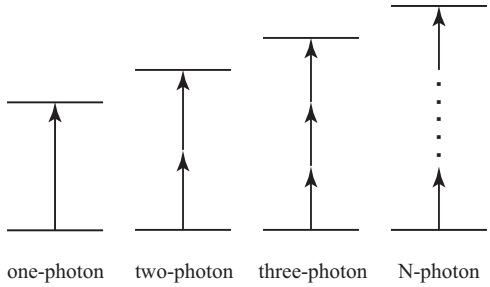

FIGURE 7.12 Illustration of one-photon and multi-photon absorption processes.

in Figure 7.12. Multiphoton absorption processes are important for a number of reasons, including the fact that multiphoton absorption constitutes a nonlinear loss mechanism that can limit the efficiency of certain optical interactions and also because of applications of multi-photon absorption such as the use of two-photon microscopy for biological applications [72] and 3D direct-laser writing [119–121].

Multiphoton absorption can be described theoretically by calculating the transition rate from the ground state to the final state through the use of time-dependent quantum-mechanical perturbation theory. The resulting expression is often referred to as Fermi's golden rule. This method applied to the case of two-photon absorption leads to a prediction for the value of the two-photon absorption cross section $\sigma_{ng}^{(2)}(\omega)$, which is defined such that the transition rate for transitions from level g to level n is given by

$$R_{ng}^{(2)} = \sigma_{ng}^{(2)}(\omega) I^2. \tag{7.49}$$

One finds that the two-photon cross section has the form

$$\sigma_{ng}{}^{(2)}(\omega) = \frac{1}{4n^2\varepsilon_0^2 c^2}\left|\sum_m \frac{\mu_{nm}\mu_{mg}}{h^2\left(\omega_{mg}-\omega\right)}\right|^2 2\pi\rho_f\left(\omega_{ng}=2\omega\right) \tag{7.50}$$

In this expression, μ_{nm} is the electric-dipole matrix element connecting levels n and m and $\rho_f(\omega_{ng} = 2\omega)$ is the density of states for the g to n transition evaluated at the laser frequency ω. Experimentally, two-photon cross sections are often quoted with intensities measured in units of photons $m^{-2}s^{-1}$. One finds, either from laboratory measurement [73] or from evaluation of equation (7.50), that a typical value of the two-photon cross section is

$$\bar{\sigma}_{ng}{}^{(2)} \approx 2.5\times10^{-58}\,\frac{m^4 s}{\text{photon}^2} \tag{7.51}$$

These predictions can readily be extended to higher-order multi-photon transition rates.

7.14 Optically Induced Damage

A topic of great practical importance is laser-induced damage of optical materials. Laser-induced damage is important because this process limits the maximum amount of optical power that can be transmitted through a given material and, consequently, limits the efficiency of many nonlinear optical interactions. The field of optical damage has been described in several review articles [74–77]; several investigations of optical damage include the following references [78,79]. There are several different mechanisms that lead to optical damage. In brief summary, these mechanisms are as follows:

- Linear absorption, leading to localized heating and cracking of the optical material. This is the dominant damage mechanism for continuous-wave and long-pulse ($\gtrsim 1$ μs) laser beams.
- Avalanche breakdown, which is the dominant mechanism for pulsed lasers (shorter then $\lesssim 1$ μs) for intensities in the range 10^{13}–10^{16}/W m^{-2}.
- Multiphoton ionization or dissociation of the optical material, which is the dominant mechanism for intensities in the range 10^{16}–10^{20} W m^{-2}.
- Direct (single cycle) field ionization, which is the dominant mechanism for intensities $> 10^{20}$ W m^{-2}.

This summary suggests that the avalanche breakdown mechanism is the dominant optical damage mechanism for laser pulses most often encountered in the laboratory and in applications. The nature of this mechanism is that a small number of free electrons initially present within the optical material are accelerated to high energies through their interaction with the laser field. These electrons can then impact-ionize other atoms within the material, thereby producing additional electrons which are subsequently accelerated by the laser field and eventually producing still more electrons. Some fraction of the energy imparted to each electron will lead to a localized heating of the material, which can eventually lead to damage of the material due to cracking or melting. A small number of electrons initially present within the material are created by one of several processes, including thermal excitation multi-photon excitation, or free electrons resulting from crystal defects.

Empirical evidence shows that, for many materials and for laser pulse lengths τ in the range of 10 ps to 100 ns, the threshold fluence for laser damage increases with pulse duration as $\tau^{1/2}$, and consequently, the threshold intensity decreases with pulse duration as $\tau^{-1/2}$. Results for the case of fused silica are shown in Table 7.7.

7.15 Strong-field Effects and High-order Harmonic Generation

Recent advances have led to the development of lasers that can produce pulses of a fraction of a femtosecond in duration. New nonlinear optical phenomena become accessible with these short laser pulses for two different reasons: (i) ultrashort laser pulses of only modest energy can produce super-intense fields; and (ii) nonlinear optical self-action effects are qualitatively different when excited by such short pulses, because of the dominance of dispersive and space-time coupling effects. Some of these new features are reviewed in the present section.

TABLE 7.7

Optical Damage Threshold of Fused Silica[a]

Pulse Duration	Threshold Fluence (kJ m^{-2})	Threshold Intensity (GW m^{-2})	Comments
1 ps	13	1.3×10^7	Deviation from $\tau^{1/2}$ scaling
10 ps	41	4.1×10^6	
100 ps	130	1.3×10^6	
1 ns	410	4.1×10^5	
10 ns	1300	1.3×10^5	
100 ns	4100	4.1×10^4	

[a] From Stuart *et al*. [78] and other sources.

Let us first consider how nonlinear optical effects are modified when excited by a super-intense pulse. nonlinear optical effects have historically been modelled using the power-series expansion of equation (7.1), but this series is not expected to converge if the laser field strength E exceeds the atomic unit of field strength $E_{at} = m^2e^5/\hbar^4 = 5.14 \times 10^{11}$ V m^{-1}. This field strength corresponds to a laser intensity of $I_{at} = 4 \times 10^{20}$ W m^{-2}, which constitutes the threshold field-strength for exciting non-perturbative nonlinear optical response.

One of the dramatic consequences of excitation with intensities comparable to the atomic unit of intensity I_{at} is the occurrence of high-harmonic generation [80,81]. In brief, if an atomic gas jet is irradiated by high-intensity laser radiation, it is observed that all odd harmonics of the laser frequency, up to some maximum value N_{max}, are emitted. The various harmonics below N_{max} are typically emitted with approximately equal intensity; such an observation is incompatible with a perturbative explanation of this phenomenon. Harmonic generation with N_{max} as large as 341 has been demonstrated.

This phenomenon can be understood in terms of a simple physical model [82]. One imagines an atomic electron that has received kinetic energy from the laser field and is excited to a highly elliptical orbit. The positively charged atomic nucleus is at one focus of this ellipse, and each time the electron passes near the nucleus, it undergoes violent acceleration and emits a short pulse of radiation. This radiation is in the form of a train of short pulses; the spectrum of the radiation is the square of the Fourier transform of this pulse train, which contains the harmonics of the oscillation period up to some maximum frequency that is approximately the inverse of the time the electron spends near the atomic core. This argument can be made qualitative to show that the maximum harmonic number is given by

$$N_{max}\hbar\omega = 3.17K + U_p \tag{7.52}$$

where $K = e^2E^2/m\omega^2$ is the 'ponderomotive energy' (the kinetic energy of an electron in a laser field) and U_p is the ionization energy of the atom.

Nonlinear optical self-action effects are also profoundly modified through excitation with ultrashort laser pulses. New phenomena come into play, including self-steepening of the laser pulse and space time focusing effects, in which different spectral components of the laser pulse undergo differing amounts of self-focusing. These effects have been described by a nonlinear envelope equation [83] which is a generalization of equation (7.38) and have been studied extensively by Gaeta [84] in the context of super-continuum generation.

REFERENCES

1. Lewis G N, Lipkin D and Magel T T 1941 *J. Am. Chem. Soc*. **63** 3005.
2. Boyd R W, Raymer M G and Narducci L M (ed) 1986 *Optical Instabilities* (Cambridge: Cambridge University Press).
3. Spence D E, Kean P N and Sibbett W 1991 *Opt. Lett*. **16** 42. Sibbett W Gran R S and Spence D E 1994 *Appl. Phys.—Lasers Opt. B* **58** 171.
4. Bloembergen N 1964 *Nonlinear Optics* (New York: Benjamin).
5. Boyd R W 2020 *Nonlinear Optics*, 4th ed. (San Diego, CA: Academic Press).
6. Butcher P N and Cotter D 1990 *The Elements of Nonlinear Optics* (Cambridge: Cambridge University Press).
7. Hannah D C, Yuratich M A and Cotter D 1979 *Nonlinear Optics of Free Atoms and Molecules* (Berlin: Springer).
8. Shen Y R 1984 *The Principles of Nonlinear Optics* (New York: Wiley).
9. Sutherland R L 1996 *Handbook of Nonlinear Optics* (New York: Dekker).
10. Agrawal G P and Boyd R W (ed) 1992 *Contemporary Nonlinear Optics* (Boston, MA: Academic).
11. Boyd R W 1996 *Laser Sources and Applications* ed A Miller and D M Finlayson (Scottish Universities Summer School in Physics) (Bristol: IOPP).
12. Boyd R W 1999 *J. Mod. Opt*. **46** 367.
13. Günter P and Huignard J-P (ed) 1988 *Photorefractive Materials and Their Applications Vols 1 and 2* (Topics in Applied Physics 61 and 62) (New York: Springer).
14. D D Nolte (ed) 1995 *Photorefractive Effects and Materials* (Dordrecht: Kluwer).
15. Prasad P N and Williams D J 1991 *Introduction of Nonlinear Optical Effects in Molecules and Polymers* (New York: Wiley).
16. Chemla D S and Zyss J 1987 *Nonlinear Optical Properties of Organic Molecules and Crystals Vols 1 and 2* (Orlando, FL: Academic).
17. Boyd R W and Fischer G L 2001 Nonlinear optical materials *Encyclopedia of Materials, Science and Technology* (Amsterdam: Pergamon) 6237–44.

18. Cleveland Crystals, Inc, 19306 Redwood Road, Cleveland, Ohio 44110 USA provides a large number of useful data sheets which may also be obtained at http://www.cleveland-crystals.com.
19. Smith A V maintains a public domain nonlinear optics data base SNLO, which can be obtained at http://www.sandia.gov/imrl/XWEB1128/xxtal.htm
20. Chase L L and van Stryland E W 1995 *CRC Handbook of Laser Science and Technology* (Boca Raton, FL: Chemical Rubber Company) section 8.1 (This reference provides an extensive tabulation of third-order nonlinear optical susceptibilities. The values of $\chi^{(3)}$ given in this reference need to be multiplied by a factor of four to conform with the standard convention of Bloembergen, which is the convention used in the present article.)
21. Hache F, Ricard D, Flytzanis C and Kreibig U 1988 *Appl. Phys. A* **47** 347.
22. Sipe J E and Boyd R W 1992 *Phys. Rev. A* **46** 1614; Boyd R W and Sipe J E 1994 *J. Opt. Soc. Am. B* **11** 297; Fischer G L, Boyd R W, Gehr R J, Jenekhe S A, J E Osaheni J A, Sipe and Weller-Brophy L A 1995 *Phys. Rev. Lett.* **74** 1871.
23. Nelson R L and Boyd R W 1999 *Appl. Phys. Lett.* **74** 2417.
24. Chase L L and van Stryland E W 1995 *CRC Handbook of Laser Science and Technology* (Boca Raton, FL: Chemical Rubber Company) section 8.1
25. Bloembergen N et al. 1969 *Opt. Commun.* **1** 195.
26. Vogel EM et al. 1991 *Phys. Chem. Glasses* **32** 231.
27. Hall D W et al. 1989 *Appl. Phys. Lett.* **54** 1293.
28. Lawrence B L et al. 1994 *Electron. Lett.* **30** 447.
29. Carter G M et al. 1985 *Appl. Phys. Lett.* **47** 457.
30. Molyneux et al. S 1993 *Opt. Lett.* **18** 2093.
31. Erlich J E et al. 1993 *J. Mod. Opt.* **40** 2151.
32. Sutherland R L 1996 *Handbook of Nonlinear Optics* (New York: Dekker) ch 8.
33. Pennington D M et al. 1989 *Phys. Rev. A* **39** 3003.
34. Euler H and Kockel B 1935 *Naturwiss.* **23** 246.
35. Hau LV et al. 1999 *Nature* **397** 594.
36. Kramer M A, Tompkin W R and Boyd R W 1986 *Phys. Rev. A* **34** 2026.
37. Franken P A, Hill A E, Peters C W and Weinreich G 1961 *Phys. Rev. Lett.* **7** 118.
38. Midwinter J E and Warner J 1965 *Brit. J. Appl. Phys.* **16** 1135
39. Armstrong J A, Bloembergen N, Ducuing J and Pershan P S *Phys. Rev.* **127** 1918.
40. Boyd G D and Kleinman D A 1968 *J. Appl. Phys.* **39** 3597.
41. Ward J F and New G H C 1969 *Phys. Rev.* **185** 57.
42. Miles R B and Harris S E 1973 *IEEE J. Quantum Electron.* **QE- 9** 470.
43. Craxton R S 1980 *Opt. Commun.* **34** 474; Seka W, Jacobs S D, Rizzo J E, Boni R and Craxton R S 1980 *Opt. Commun.* **34** 469.
44. Giordmaine J A and Miller R C 1965 *Phys. Rev. Lett.* **14** 973; Giordmaine J A and Miller R C 1966 *Appl. Phys. Lett.* **9** 298.
45. Smith R G et al. 1968 *Appl. Phys. Lett.* **12** 308.
46. Bosenberg W R, Pelouch W S and Tang C L 1989 *Appl. Phys. Lett.* **55** 1952.
47. Byer R L and Herbst R L 1977 *Tunable Infrared Generation* ed Y R Shen (Berlin: Springer).
48. Zel'dovich B Ya, Popovichev V I, Ragulsky V V and Faizullov F S 1972 *JETP Lett.* **15** 109.
49. Zel'dovich B Ya, Pilipetsky N F and Shkunov V V 1985 *Principles of Phase Conjugation* (Berlin: Springer).
50. Fisher R A 1983 (ed) *Optical Phase Conjugation* (Orlando, FL: Academic).
51. Boyd R W and Grynberg G 1992 *Contemporary Nonlinear Optics* ed G P Agrawal and R W Boyd (Boston, MA: Academic).
52. Gauthier D J, Boyd R W, Jungquist R K, Lisson J B and Voci L L 1989 *Opt. Lett.* **14** 325.
53. Gaeta A L and Boyd R W 1988 *Phys. Rev. Lett.* **60** 2618.
54. Svelto O 1974 *Progress in Optics* vol XII, ed E Wolf (Amsterdam: North-Holland).
55. Blair S, Wagner K and McLeod R 1994 *Opt. Lett.* **19** 1943.
56. Bespalov V I and Talanov V I 1966 *JETP Lett.* **3** 307.
57. Maillotte H, Monneret J and Froehly C 1990 *Opt. Commun.* **77** 241.
58. Jain M, Xia H, Yin G Y, Merriam A J and Harris S E 1996 *Phys. Rev. Lett.* **77** 4326.
59. Zakharov V E and Shabat A B 1972 *Sov. Phys.–JETP* **34** 62.
60. Mollenauer L F, Stolen R H and Gordon J P 1980 *Phys. Rev. Lett.* **45** 1095.
61. Gibbs H M 1985 *Optical Bistability* (Orlando, FL: Academic).
62. Gibbs H M, McCall S L and Venkatesan T N 1976 *Phys. Rev. Lett.* **36** 113.
63. Lugiato L A 1984 'Theory of optical bistability' *Progress in Optics* vol XXI, ed E Wolf (Amsterdam: North-Holland).
64. Szöke A, Daneu V, Goldhar J and Kurnit N A 1969 *Appl. Phys. Lett.* **15** 376.
65. Stegeman G I and Miller A 1993 *Photonics in Switching* (San Diego, CA: Academic).
66. Gibbs H M, Khitrova G and Peyghambarian N (ed) 1990 *Nonlinear Photonics* (Berlin: Springer).
67. Fabelinskii I L 1986 *Molecular Scattering of Light* (New York: Plenum).
68. Hellwarth R W 1963 *Phys. Rev.* **130** 1850.
69. Kaiser W and Maier M 1972 *Laser Handbook* ed F T Arechi and E O Schulz-DuBois (Amsterdam: North-Holland).
70. Simon U and Tittel F K 1994 *Methods of Experimental Physics* vol III, ed R G Hulet and F B Dunning (Orlando, FL: Academic).
71. Garmire E, Pandarese F and Townes C H 1963 *Phys. Rev. Lett.* **11** 160.
72. Denk W, Strickler J H and Webb W W 1990 *Science* **248** 73; Xu C and Webb W W *1997 Topics in Fluorescence Spectroscopy, Volume 5: Nonlinear and Two-Photon-Induced Fluorescence* ed J Lakowicz (New York: Plenum) ch 11.
73. Xu C and Webb W W 1996 *J. Opt. Soc. Am. B* **13** 481.
74. Bloembergen N 1974 *IEEE J. Quantum Electron.* **10** 375.
75. Lowdermilk W H and Milam D 1981 *IEEE J. Quantum Electron.* **17** 1888.
76. Raizer Y P 1965 *Sov. Phys.–JETP* **21** 1009.
77. Manenkov A A and Prokhorov A M 1986 *Sov. Phys.–Usp.* **29** 104.
78. Stuart B C et al. 1995 *Phys. Rev. Lett.* **74** 2248; Stuart B C et al. 1996 *Phys. Rev. B* **53** 1749.
79. Du D et al. 1994 *Appl. Phys. Lett.* **64** 3071.

80. Ferray M et al. *1988 J. Phys. B* **21** L31.
81. Chang Z et al. 1997 *Phys. Rev. Lett.* **79** 2967.
82. Corkum P B 1993 *Phys. Rev. Lett.* **71** 1994.
83. Brabec T and Krausz F 1997 *Phys. Rev. Lett.* **78** 3282.
84. Gaeta A L 2000 *Phys. Rev. Lett.* **84** 3583.
85. Reshef O 2017 *Opt. Lett.* **42** 3225.
86. Maier S A 2007 *Plasmonics: Fundamentals and Applications* (New York, NY: Springer).
87. Ozbay E 2006 *Science* **311** 189.
88. Berini P 2009 *Adv. Opt. Photonics* **1** 484.
89. Lee J et al. 2014 *Nature* **511** 65.
90. Li G et al. 2017 *Nat. Rev. Mater.* **2** 17010.
91. Alam M Z et al. 2018 *Nat. Photonics* **12** 79.
92. Fröhlich H 1968 *Theory of Dielectrics: Dielectric Constant and Dielectric Loss* (Oxford: Oxford University Press).
93. Bohren C E and Huffman D R 1998 *Absorption and Scattering of Light by Small Particles* (Weinheim, Germany: Wiley-VCH Verlag GmbH).
94. Vial A et al. 2005 *Phys. Rev.* B **71** 085416.
95. Hache F et al. 1986 *J. Opt. Soc. Am. B* **3** 1647.
96. Hache F et al. 1988 *App. Phys.* A **47** 347.
97. Boyd R W, Shi Z and De Leon I 2014 *Optics Comm.* **326** 74.
98. Clerici M et al. 2017 *Nat. Commun.* **8** 15829.
99. Qian H, Xiao Y and Liu Z 2016 *Nat. Commun.* **7** 13153.
100. Ginzburg P et al. 2010 *Opt. Lett.* **35** 1551.
101. Alam M Z, De Leon I and Boyd R W 2016 *Nat. Photonics* **352** 795.
102. Ricard D, Roussignol P and Flytzanis C 1985 *Opt. Lett.* **10** 511.
103. Vogel E M, Weber M J and Krol D 1991 *Phys. Chem. Glasses* **32** 231.
104. Bloembergen N, Burns W K and Matsuoka M 1969 *Optics Comm.* **1** 195.
105. Smith D D et al. 1999 *J. Appl. Phys.* **86** 6200.
106. De Leon I et al. 2014 *Opt. Lett.* **39** 2274.
107. Ila D et al. 1998 *Nucl. Instr. Meth. Phys. Res. B* **141** 289.
108. Fukumi K et al. 1991 *Jpn J. Appl. Phys.* **30** L742.
109. Haglund R F et al. 1992 *Nucl. Instr. Meth. Phys. Res. B* **65** 405.
110. Haglund R F et al. 1993 *Opt. Lett.* **18** 373.
111. Mazzoldi P et al. 1996 *J. Nonlinear Opt. Phys. Mater.* **5** 285.
112. Huang H H et al. 1997 *Langmuir* **13** 172.
113. Falconieri M et al. 1998 *Appl. Phys. Lett.* **73** 288
114. Caspani L et al. 2016 *Phys. Rev. Lett.* **116** 233901.
115. Elim H I, Ji W and Zhu F 2006 *Appl. Phys. B* **82** 439.
116. Sheik-Bahae M, Said A A and Van Stryland E W 1989 *Optics Lett.* **14** 955.
117. Sheik-Bahae M et al. 1990 *IEEE J. Quantum Electron* **26** 760.
118. Rong H et al. 2005 *Nature* **433** 725.
119. Maruo S, Nakamura O and Kawata S 1997 *Opt. Lett.* **22** 132.
120. Kawata S et al. 2001 *Nature* **412** 697.
121. Vora K et al. 2012 *Appl. Phys. Lett.* **100** 063120.